



We are Nitinol.™

## **Finite Element Analysis on Nitinol Medical Devices**

Xiao-Yan Gong and Alan R. Pelton

Proceedings of SMST-2003, Monterey, CA, eds., A.R. Pelton and T.W. Duerig, 443-451  
(2004).

2004

# SMST-2003

*Proceedings of the International Conference on*

## **Shape Memory and Superelastic Technologies**

*5 May to 8 May 2003*

*Asilomar Conference Center*

*Pacific Grove, California, USA*

### **Editors**

**Alan R. Pelton**

**Tom Duerig**



© 2004 by SMST  
All rights reserved.

No part of this book may be reproduced, stored in a retrieval system, or transcribed, in any form or by any means—electronic, mechanical, photocopying, recording, or otherwise—without prior permission of the publisher.

Published by:  
SMST Society, Inc.  
c/o SRI M/S AA287  
333 Ravenswood Avenue  
Menlo Park, California 94025  
USA  
Telephone: (650) 879-6476  
E-mail: info@smst.org  
Website: www.smst.org

Copies of this book may be ordered through the SMST website at [www.smst.org](http://www.smst.org) or by calling the SMST office at (650) 859-6476, or through ASM International, Customer Service at (440) 338 5151 x5537 or at [www.asminternational.org](http://www.asminternational.org).

Printed and bound in the United States of America

**Library of Congress Control Number: 2004102781**

**Publisher's Cataloging in Publication Data**

SMST-2003: proceedings of the international conference on shape memory and superelastic technologies / edited by Alan R. Pelton and Tom Duerig.

xvi; 746 p.; 26 cm

Includes bibliographical references and index.

ISBN 0-9660508-3-5

1. Alloys—Congresses. 2. Alloys—Thermomechanical properties. 3. Shape memory effect. I. Pelton, Alan (Alan R.) II. Duerig, Tom (Thomas W.)

TN690.S675                      2004  
669'.94—dc20

\*\*\*

Production Services by TIPS Technical Publishing, Inc.

# FINITE ELEMENT ANALYSIS AND EXPERIMENTAL EVALUATION OF SUPERELASTIC NITINOL STENT

Xiao-Yan Gong,<sup>1</sup> Alan R. Pelton,<sup>1</sup> Tom W. Duerig,<sup>1</sup> Nuno Rebelo,<sup>2</sup> and Ken Perry<sup>3</sup>

<sup>1</sup>*Nitinol Devices & Components, 47533 Westinghouse Drive, Fremont, CA 94539*

<sup>2</sup>*ABAQUS West, 39221 Paseo Padre Parkway #F, Fremont, CA, 94538*

<sup>3</sup>*EchoBio, 579 Azalea Avenue NE, Bainbridge Island, WA 98110*

## ABSTRACT

The mechanical properties of Nitinol stents are normally evaluated experimentally due to complexities resulting from large deformations and material nonlinearity. Despite difficulties associated with Finite Element Analysis (FEA), the success of computational analysis in combination with experimental study leads to better understanding of stent performance. This paper compares experimentally evaluated radial resistive forces of a Nitinol stent to predictions based on nonlinear FEA. The FEA was performed using ABAQUS with two user material subroutines independently developed specifically for Nitinol. Close agreements between the FEA and the experiments are shown for both user material subroutines.

## KEYWORDS

NiTi, Finite Element Analysis, Superelastic, Crush, Stent, Radial Stiffness

## INTRODUCTION

Recently, Finite Element Analysis (FEA) on Nitinol has been improved to cover superelastic behavior and has been proven to be a successful prediction tool in device design [1–6]. Among many successful applications, Nitinol self-expanding stents have drawn much attention. Compared to a balloon-expandable stent, a Nitinol self-expanding stent can be designed to provide constant gentle outward pressure, yet maintain high resistance to inward pressure and high crush resistance, in addition to its ease of deployment [7–8]. Because of these unique properties, demands for Nitinol self-expanding stents are increasing for certain applications.

The most important mechanical requirements for a stent are radial stiffness and fatigue life. Although both requirements can be evaluated through physical tests, they require “build-test” iterations and involve long-lasting fatigue testing. Thus, they can be very costly and time consuming. A

10-year device fatigue life under the heart rate of 75 beats per min. projects a 400 million cyclic pulsatile loading on the stent. Even with an accelerated fatigue test, a 400 million-cycle fatigue test can last months. FEA is an extremely useful complement and has proven to be effective and capable of providing a better, more detailed understanding of fatigue and design [9–10].

This paper discusses the results using two different approaches to modeling the superelastic constitutive behavior of Nitinol. Both approaches are then used in the analysis to determine the radial stiffness and crush characteristics of a Nitinol self-expanding stent. Comparisons with these tests confirm that FEA provides good predictions of the stent's mechanical response. Close agreement between two different constitutive approaches indicates FEA is a capable predictive tool in the early design phase of Nitinol devices.

## CONSTITUTIVE MODELS

It is well known that Nitinol is a thermomechanical coupled material. Pelton *et al.* systematically demonstrated this thermomechanical coupled material response [11]. In their work, uniaxial stress-strain behavior of Nitinol wires was studied from  $-100^{\circ}\text{C}$  to  $150^{\circ}\text{C}$  as shown in Figure 1. The series of stress-strain responses at different temperatures demonstrate the highly nonlinear, path and temperature dependent material constitutive behavior.

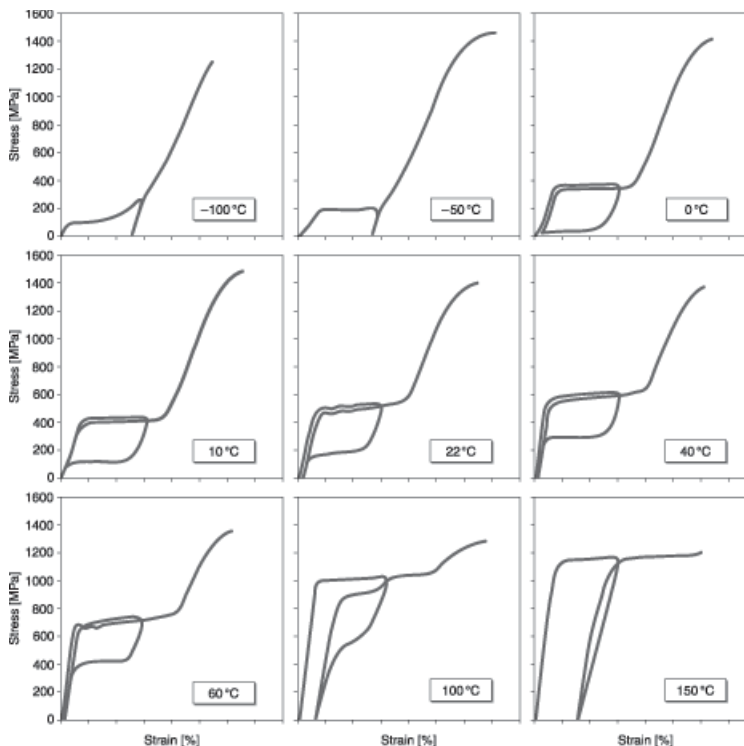


Figure 1 Uniaxial stress-strain relation at different temperatures.

Pelton *et al.* were also among the first to analyze the nonlinear material behavior of Nitinol using FEA, taking advantage of the available hyperelastic theory for rubbers [12]. This approach is very intuitive as Nitinol is, to some extent, a “rubber in the metal form.” Despite their success, hyperelas-

tic theory is known to have stability issues that require more calibration tests (namely uniaxial tension, biaxial tension, and shear) to stabilize the model. Furthermore, the hyperelastic material model does not address the path and temperature dependent material behavior of Nitinol [13].

Over the last 10 years, many theories have been developed independently to account for the nonlinear path dependent thermomechanical constitutive behaviors of Nitinol [14–18]. They build the foundation for the state-of-art constitutive description of Nitinol. To date, advanced FEA on Nitinol has adopted those theories. The two constitutive models used in this paper are based on the approaches proposed by Auricchio et al. and by Qidwai and Lagoudas respectively [16–18]. For completeness, their approaches are briefly summarized below.

Auricchio's approach is based on generalized plasticity theory [16–17]. It models superelastic behavior of Nitinol, where any strain increment is decomposed into a linear elastic part and a stress-induced transformation part. The transformation part follows standard plasticity rules, such that strain increments can be derived from a plastic potential. The model includes transformation surfaces (analogous to yield surfaces) for both the austenite-to-martensite transformation and the reverse martensite-to-austenite transformation. ABAQUS West implemented this theory with modifications to allow for different elastic properties for austenite and for martensite, as well as different transformation stresses in tension and in compression. The loading can be either mechanical or thermal, and the transformation stresses (surfaces) are temperature dependent.

Qidwai and Lagoudas have developed constitutive models for shape memory and superelastic materials based on first principles [18]. In their approach, the second law of thermodynamics is written in terms of the Gibbs free energy. Strain, temperature, and martensite volume fraction become state variables that must satisfy the second law of thermodynamics. An evolution equation for the martensite volume fraction is derived from a dissipation potential and the effective transformation surfaces are evaluated as functions of the state variables. This approach also allows for different temperature-dependant elastic properties for austenite and martensite, and accommodates both mechanical and thermal loading. EchoBio developed a user-defined material subroutine based on this theory.

Both constitutive models need calibration based on a uniaxial tensile test. Figure 2 plots the comparison of the two independently developed constitutive models and the experimental result of Nitinol tubing that has been processed to achieve an austenite finish temperature ( $A_f$ ) of 29°C and is tested at 37°C. Note that both models can be calibrated to predict the material's response well up to 8% strain based on a limited number of parameters. Discrepancy arises at higher strains because neither material model covers the plasticity in the martensitic phase. ABAQUS/Standard version 6.2-1 along with Nitinol UMAT/3D 3.24 (developed by ABAQUS West) and another user-defined material subroutine by EchoBio were used in the analyses.

## RESULTS AND DISCUSSION

### Radial Resistive Force (RRF) and Chronic Outward Force (COF)

RRF and COF are important mechanical responses unique to Nitinol Superelastic stents. RRF is the force generated by a stent to resist the reduction in its diameter and COF is the force generated by a stent when it self-expands from a smaller diameter towards a larger diameter. COF operates in the unloading portion of Nitinol's stress-strain curve while RRF operates on the loading portion of Nitinol's stress-strain curve. Generally speaking, RRF and COF are different and RRF is much larger than COF.

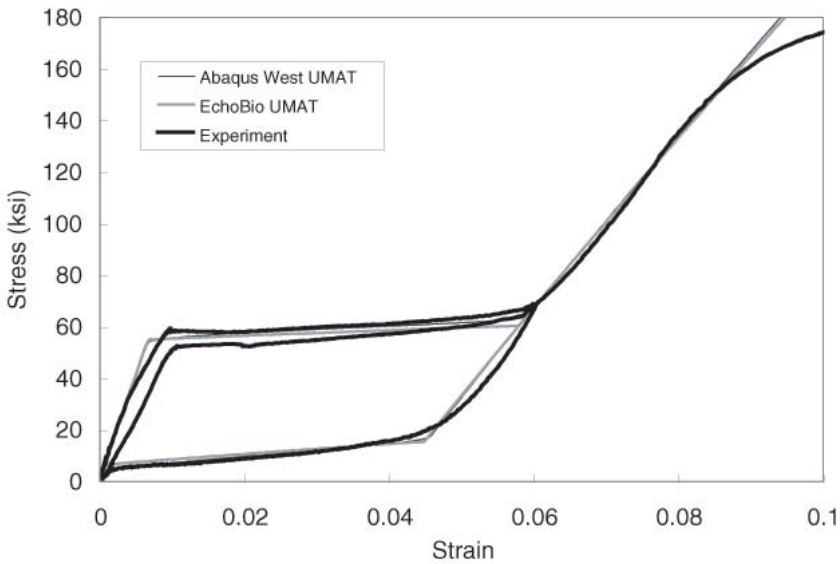


Figure 2 Comparison of FEA predictions and the experimental data.

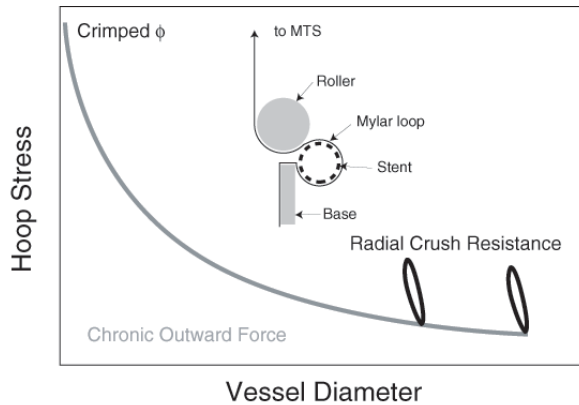


Figure 3 Schematic radial stiffness test setup.

Figure 3 illustrates schematically how these values are evaluated experimentally. Generally, this experiment is performed on an MTS system with customized test fixtures. In the first step, the stent is crimped down at a low temperature to a diameter of the delivery system. It is then placed inside the Mylar loop with one end of the loop fixed to the test fixture and another end connected to the MTS force actuator. The warm water of 37°C is then added so that the crimped stent is submerged at the constant body temperature. This causes the stent to produce an expansion radial force against the Mylar loop because the stent tends to recover back to its manufactured diameter. The Mylar loop then transfers the stent expansion force to the MTS load cell. By moving the MTS head down, one can release the pulling force and record the force as function of the head movement. The stent diameter change can be calculated based on the head movement. Thus, the force as a function of the

stent diameter is obtained. Notice that the recorded force comes from releasing the stent from its crimped diameter; therefore, it measures COF. At a given stent diameter when RRF is of interest, the MTS head is reversed to move up so that a pulling force on the Mylar is transferred to compress the stent down to a smaller diameter. This way, the RRF at this diameter is obtained. After the RRF is obtained, one can reverse the MTS head again to complete the test or can repeat the sequences to obtain the RRF at different stent diameters.

For simplicity, a two-strut model shown in Figure 4 is used in our FEA. For comparison purposes, the same model and mesh were used in the study. A 10 mm SMART Control™ stent from Cordis self-expanding stent product line is selected for the RRF and COF study. In this model, symmetrical boundary conditions are applied to the open surfaces to maintain symmetrical deformation. User-defined rigid surfaces are used to compress and release the stent to the necessary stent diameters. The artificial stability option in ABAQUS/Standard is also turned on so that the analysis can run smoothly. The total strain energy and total artificial strain are traced during the whole simulation to ensure that the artificial energy is negligible.

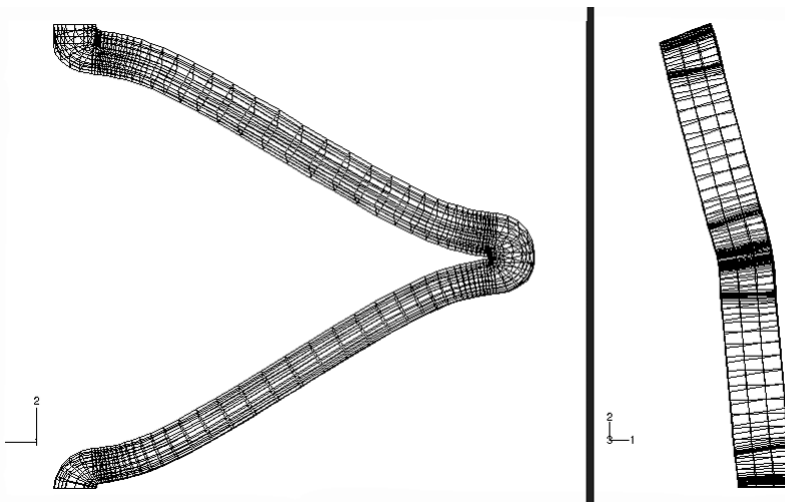


Figure 4 Side (left) and top (right) views of a two strut model.

Figure 5 shows the comparison between the FEA predictions and the test results. In both material constitutive models, the reload of the Nitinol is not simulated correctly. In addition, there are discrepancies at smaller stent diameters. This corresponds to the lack of a plasticity model at high strain in the martensitic phase in both material models; however, the COF agrees well with the experimental result at larger diameters. Luckily, larger diameters are of greater interests in stent applications. Furthermore, if one keeps in mind that RRF originates from the material response on the loading path, one can find the correct predictions of the RRF from the FEA results during the compression of the stent. Thus, even for these challenging results, the FEA solution agrees closely with the experimental results.

Figure 6 shows the strain contours on the deformed struts. The high strain locations identify the fatigue critical areas in stent manufacturing. Figure 7 plots the comparison of peak maximum principal strains for both material models. There is a close agreement between both material models and actual material behavior.

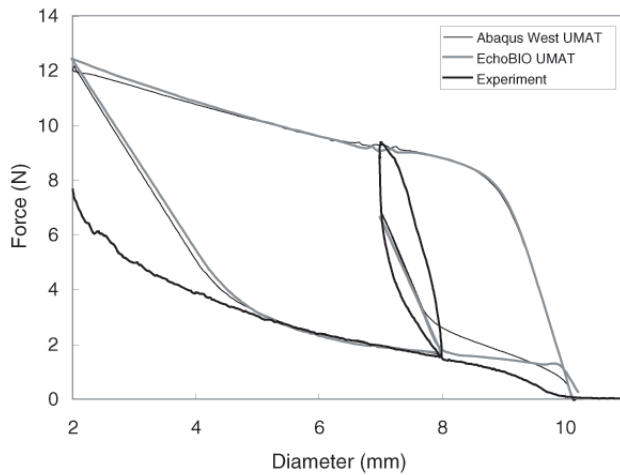


Figure 5 Comparisons of FEA predictions and the tests results.

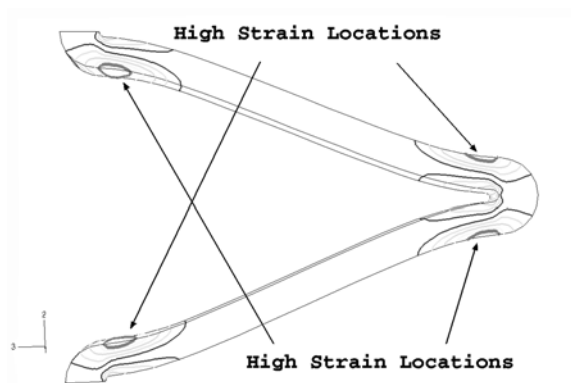


Figure 6 Maximum principal strain contours indicate the fatigue critical areas.

### Crush Resistance

The same diameter stent was chosen for the crush test. The crush test was performed on EnduraTec desktop tester ELF/3200 series, capable of higher displacement and load resolution. The test setup is straightforward. The stent was first deployed inside an 8 mm inner diameter (ID) 5% compliant tube (over 100 mmHg pressure differential) to simulate the worst case oversizing per the product IFU. The stented tube is then crushed between two rigid plates while the force and displacement were monitored. Air heating is used in this test. Environment temperature is 37° C to simulate the body temperature.

Figure 8 shows the FEA model for this simulation. Due to the repetitive patterns of a stent, only two half-row struts are used in the analysis. Axial and rotational repetitive boundary conditions are applied to the open ends of the model. The analysis involves rigid-to-flexible and flexible-to-flexible contacts over three steps. In the first step, all the contacts are removed so that the compliant tube, simulated as shell elements, is pressurized to expand to a diameter slightly larger than the stent outer diameter (OD). In the second step, the contact between the compliant tube and the stent

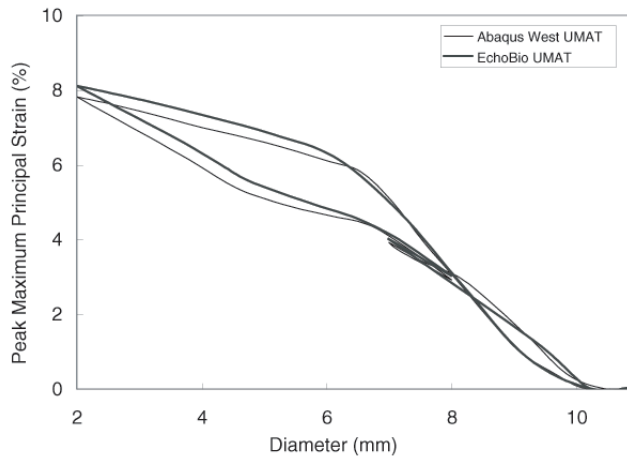


Figure 7 Peak maximum principal strain as function of stent diameter.

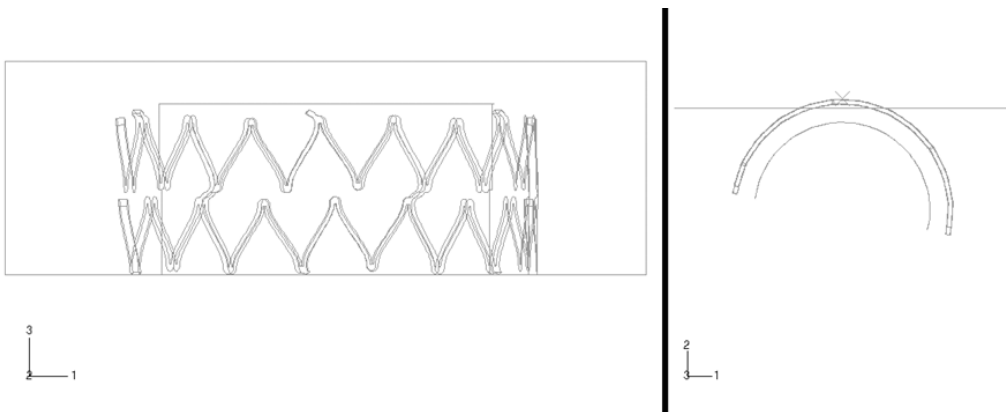


Figure 8 Side (left) and top (right) views of the FEA model for crush simulation.

OD is activated and the pressure acting on the tube ID is released completely so that the tube and stent reach their equilibrium positions. In the last step, contact between a rigid surface and the tube OD is activated so that the rigid surface can crush the stented tube. This simulation is difficult, not only due to the contacts and the material nonlinearity, but mainly because of the buckling of the stent. As a matter of fact, the buckling is visually observed both from the test and the FEA, as shown in the comparison of the deformed shapes from the experiment and the FEA in Figure 9.

Figure 10 plots the force-displacement response when the stented tube is crushed. Once again, good agreement between the FEA and the experiment indicates that both the material models represent the material response well. Yet FEA predicts lower force than actual measurement. This may be due partially to the test equipment compliance and partially to the lack of the input of the stress-strain response when Nitinol is subjected under compression. Figure 11 compares the peak maximum principal strain as function of the crush displacement for both material models. Once again, they agree closely.

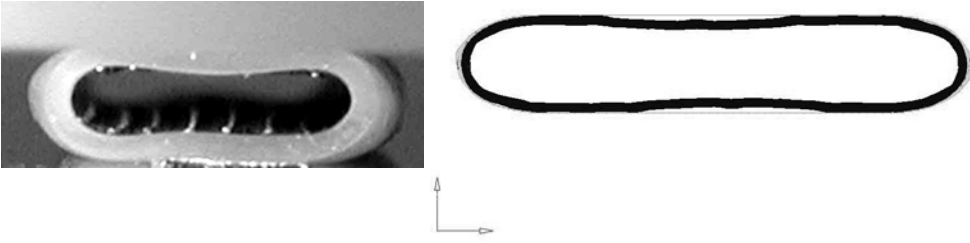


Figure 9 Comparison of deformed stent shape from experiment (left) and FEA (right).

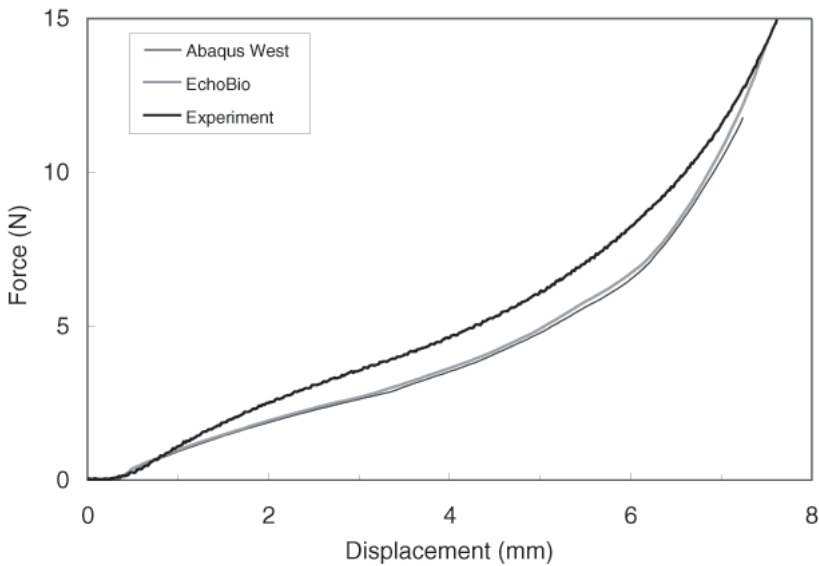


Figure 10 Comparison of force-displacement relations from experiment and FEA.

## CONCLUSIONS

We showed that FEA, based on two different user-defined material subroutines, predicts consistent mechanical response for stents. Key results from FEA done with both material models agree well with experimental results, indicating that FEA is a powerful predictive tool that can be used in product development and design. Improvement of the material constitutive models for Nitinol is necessary to accurately describe the plasticity in the martensitic phase, as well as under multiple loading and unloading sequences.

## REFERENCES

1. X. Gong and A.R. Pelton in *Proceedings of ABAQUS Users' Conference* (New Port, R.I., 2002), p. 1.
2. N. Rebelo and M. Perry, *Min. Invas. Ther. & Allied. Technol.* **9** (2) (2000), p. 75.

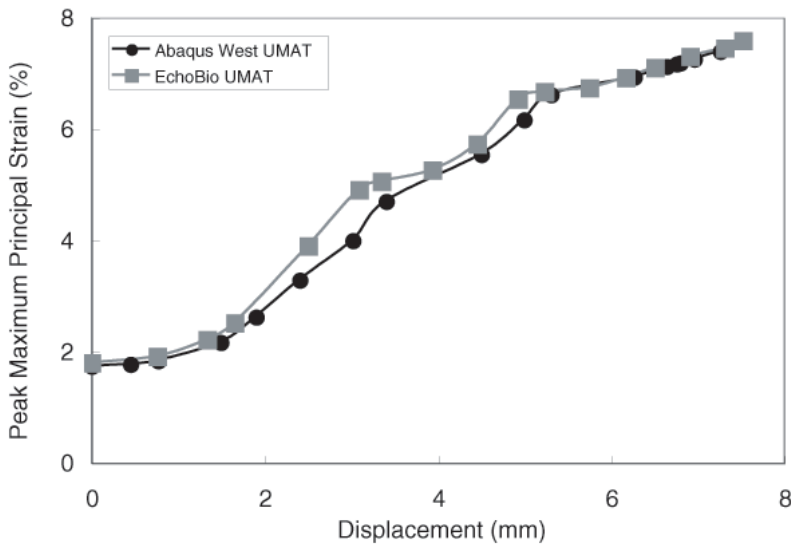


Figure 11 Peak maximum principal strain as function of displacement from two different material models.

3. N. Rebelo, M. Hsu, and H. Foadian in *SMST-2000: Proceedings of the International Conference on Shape Memory and Superelastic Technologies*, eds. S.M. Russell and A.R. Pelton (Pacific Grove, Calif.: International Organization on SMST, 2000), p. 495.
4. E. Patoor, Y. Gillett, E. Segard, and M. Berveiller in *SMST-97: Proceedings of the Second International Conference on Shape Memory and Superelastic Technologies*, eds. A.R. Pelton, D. Hodgson, S. Russell, and T.W. Duerig (Pacific Grove, Calif.: International Organization on SMST, 1997), p. 35.
5. F. Trochu and P. Terriault in *SMST-97: Proceedings of the Second International Conference on Shape Memory and Superelastic Technologies*, eds. A.R. Pelton, D. Hodgson, S. Russell, and T.W. Duerig (Pacific Grove, Calif.: International Organization on SMST, 1997), p. 595.
6. M.D. Perry and R.T. Chang in *SMST-97: Proceedings of the Second International Conference on Shape Memory and Superelastic Technologies*, eds. A.R. Pelton, D. Hodgson, S. Russell, and T.W. Duerig (Pacific Grove, Calif.: International Organization on SMST, 1997), p. 601.
7. T.W. Duerig and M. Wholey, *Min. Invas. Ther. & Allied. Technol.* **11** (4) (2002), p. 173.
8. T. Duerig, D.E. Tolomeo, and M. Wholey, *Min. Invas. Ther. & Allied. Technol.* **9** (3/4) (2000), p. 235.
9. D. Tolomeo, S. Davidson, and M. Santinoranont in *SMST-2000: Proceedings of the International Conference on Shape Memory and Superelastic Technologies*, eds. S.M. Russell and A.R. Pelton (Pacific Grove, Calif.: International Organization on SMST, 2000), p. 471.
10. C. Kugler, D. Maston, and K. Perry in *SMST-2000: Proceedings of the International Conference on Shape Memory and Superelastic Technologies*, eds. S.M. Russell and A.R. Pelton (Pacific Grove, Calif.: International Organization on SMST, 2000), p. 409.

11. A.R. Pelton, J. Dicello, and S. Miyazaki, *Min. Invas. Ther. & Allied. Technol.* **9** (2) (2000), p. 107.
12. A.R. Pelton, N. Rebelo, T.W. Duerig, and A. Wick in *SMST-94: Proceedings of the First International Conference on Shape Memory and Superelastic Technologies*, eds. A.R. Pelton, D. Hodgson, and T.W. Duerig (Pacific Grove, Calif.,1994), p. 353.
13. M. Pease and B. Walsh in *SMST-2000: Proceedings of the International Conference on Shape Memory and Superelastic Technologies*, eds. S.M. Russell and A.R. Pelton (Pacific Grove, Calif.: International Organization on SMST, 2000), p. 495.
14. R. Abeyaratne and J. Knowles, *J. Mech. Phys. Solids* **41** (1993), p. 541.
15. L. Anand and M. Kothari, *J. Mech. Phys. Solids* **44** (1996), p. 525.
16. F. Auricchio and R. Taylor, *Comput. Methods. Appl. Mech. Engng.* **143** (1996), p. 175.
17. F. Auricchio and R. Taylor, *Comput. Methods. Appl. Mech. Eng.* **146** (1997), p. 281.
18. M.A. Qidwai and D.C. Lagoudas, *Int. J. Numer. Meth. Engng.* **46** (2000), p. 1123.